Journal of Drug Delivery Science and Technology 90 (2023) 104977

Contents lists available at ScienceDirect

Journal of Drug Delivery Science and Technology

journal homepage: www.elsevier.com/locate/jddst

FUS and surfactant-based nanocarriers: A combined strategy for nose to brain drug delivery

Nunzia Maisto [a,b], Dalila Mango [b,d], Andrea Bettucci [c], Gaetano Barbato [d,e,**], Maria Grazia Ammendolia [f], Federica Rinaldi [g,*], Carlotta Marianecci [g], Robert Nisticò [b,d,1], Maria Carafa [g,1]

[a] Department of Physiology and Pharmacology "V. Erspamer", Sapienza University of Rome, Rome, Italy
[b] Laboratory of Neuropharmacology, EBRI Rita Levi-Montalcini Foundation, Rome, Italy
[c] Department of Basic and Applied Sciences for Engineering, Sapienza University of Rome, Via A. Scarpa 16, 00185, Rome, Italy
[d] School of Pharmacy, Department of Biology, University of Rome Tor Vergata, Rome, Italy
[e] Inno-Sol srl, Rome, Italy
[f] National Centre for Innovative Technologies in Public Health, Istituto Superiore di Sanità, 00161, Rome, Italy
[g] Department of Drug Chemistry and Technology, Sapienza University of Rome, Rome, Italy

ARTICLE INFO

Keywords:
Niosomes
Nanobubbles
Nose to brain
Drug delivery
Ultrasound contrast agents
Synaptic plasticity

ABSTRACT

Brain drug delivery is hampered by the presence of the blood brain barrier and nanocarriers, administered by intranasal route, could represent an alternative and efficient strategy to improve drug localization in the Central Nervous System (CNS). The aim of this work is to design and characterize non-ionic surfactant vesicles (NSVs) and perfluorocarbon gas non-ionic surfactant based nanobubbles (VNBs) suitable for Nose to Brain Delivery (N2B). In particular, Pluronic F127, Span 85 and cholesterol have been employed to prepare NSVs and VNBs. Both systems have been characterized in terms of (a) hydrodynamic diameter, ζ-potential and morphology (b) vesicle bilayer feature (anisotropy), (c) physical-chemical stability and (d) fluorescent model probe release capability. VNBs have been also studied in terms of gas entrapment and acoustic efficiency. In addition, in order to understand optimal ultrasound (US) parameters to obtain *in vitro* stable cavitation, the acoustic pressure effect on VNBs fluorescent probes release kinetics was evaluated. The obtained results suggest that NSVs and VNBs show a hydrodynamic diameter suitable for N2B delivery. Moreover, in this study, we develop a new kind of protocol to evaluate an *in vitro* US characterization of VNBs and our data suggest a stable and controlled probe release, encouraging the possibility to deliver VNBs in mixture with NSVs loaded neuroprotective drugs for brain delivery coupled to US obtaining stable cavitation. In this context, extracellular field recordings in specific area of hippocampus (CA1-CA3) have been carried out in order to assure that empty NSVs do not affect synaptic plasticity in the form of long-term potentiation, a molecular mechanism which underlies learning and memory.

1. Introduction

Disorders of the central nervous system (CNS) represent an important health issue of disability and are leading to additional medical treatment and prolonged care; especially neurodegenerative disorders are becoming relevant with the increasing age of the population [1]. Neurodegenerative diseases are often associated with atrophy of the affected central or peripheral structures of the nervous system, a decline in neurological function and neuronal death. In the set of disorders of CNS, Alzheimer's disease is the most prevalent of the neurodegenerative diseases followed by Parkinson's disease. A minor number of patients are affected by amyotrophic lateral sclerosis and Huntington's diseases which have negative consequences [2]. In that regard, the main problem is related to the inadequacy of current therapeutic strategies, which are meant to alleviate the symptoms without any disease-modifying effect. Interestingly, novel treatments as biological therapeutics based on

* Corresponding author.
** Corresponding author. Inno-Sol srl, Rome, Italy.
E-mail addresses: gaetano.barbato@inno-sol.it (G. Barbato), federica.rinaldi@uniroma1.it (F. Rinaldi).
[1] These authors contributed equally to this work.

https://doi.org/10.1016/j.jddst.2023.104977
Received 27 June 2023; Received in revised form 6 September 2023; Accepted 17 September 2023
Available online 29 September 2023

peptides, proteins, and nucleic acid, hold the disease modifying potential but they could have several pharmacokinetic problems, including bioavailability, as the presence of the blood brain barrier (BBB) hinders the brain targeting.

BBB challenges brain drug delivery due to its structure characterized by tight junctions limiting paracellular and *trans*-cellular permeability and transport [3,4]. Consequently, BBB plays an important role to protect the brain and to regulate the afflux of substances; same small lipophilic molecules are able to passively diffuse while some small hydrophilic molecules cross the BBB using paracellular pathway. Nevertheless, approximately 98% of all small molecules and almost all large molecules, are unable to cross the BBB and to reach the CNS [5,6]. In this context, nose to brain drug delivery (N2B) is a non-invasive approach for transporting drugs from the nose directly into the brain through the unique olfactory and trigeminal neural pathways that connect the nasal mucosa with the perivascular spaces within the CNS [7,8].

Traditionally, N2B delivery is employed to promote local effects such as the treatment of rhinitis or allergy. However, due to its many favourable characteristics, including non-invasiveness, good patient compliance, and ease of administration, N2B administration might be used to obtain an effective brain delivery [9]. Unfortunately, N2B access presents challenges and obstacles, like low delivery efficiency due to mucosal clearance and nasal absorption, and rapid/widespread distribution throughout the brain resulting in non-focal delivery [10,11]. In this regard, N2B delivery by "soft" nanocarriers, such as liposomes or niosomes, represent a promising non-invasive alternative to overcome challenges presented by the N2B route. N2B nano-based drug delivery systems have been demonstrated to improve drug permeability and absorption, drug uptake in the olfactory region, and their access and distribution into the brain. At the same time, they can protect therapeutic agents from degradation and prevent their extracellular transport by outgoing transporters [12]. Moreover, the use of N2B nanoparticle system combined with other techniques, such as intensity focused ultrasound (FUS), could enable a higher degree of selective drug delivery to the brain.

FUS is currently the most advanced and viable method to permeabilize the BBB transiently and non-invasively [13]. Especially, FUS, in conjunction with intravenously (IV) injected gas-encasing and stabilizing outer shell microbubbles, can non-invasively and transiently permeabilize the BBB, hence greatly enhancing CNS delivery of drugs after their systemic or intranasal administration [14,15]. However, IV administration can induce serious adverse effects. An alternative and valid approach might be coupling FUS and microbubbles N2B delivery [16,17]. Nevertheless, due to their size (1–5 μm), microbubbles cannot extravasate from intravascular into interstitial space and their size remains one of the major limitations to their administration. Nano-sized bubbles can potentially overcome this impasse and they could potentially enhance the permeability of drugs through BBB [18].

The aim of this work is to design and characterize non-ionic surfactant vesicles (NSVs), known as niosomes, suitable for N2B delivery, able to load and deliver the model fluorescent probe. Niosomes are drug delivery systems, similar to liposomes, and they are able to encapsulate both hydrophilic and lipophilic drugs. The low surfactant cost, the greater stability, and the resultant ease of storage have led to the development of these carriers as alternatives to liposomes. In the meantime, using the same niosomes components, vesicular nano-size bubbles (VNBs) have been prepared in order to entrap gas. The VNBs could be administered by N2B route, together with drug loaded NSVs to improve the drug localization in the CNS [19]. This represents an innovative and unusual approach in fact, by scopus research 1390 documents from 2000 to 2024 have been published on the N2B delivery topic, but only 7 papers have been published on to N2B drug delivery-bubbles, and this suggests that the topic of this research paper is an innovative approach worthy to be investigated.

Based on a previous study carried out by Hanieh et al., 2022 [18], VNBs were filled with perfluorocarbon gas (PFC), that is biocompatible, inert, chemically highly stable and not metabolized in the body after injection [18,20].

To obtain stable vesicular systems, several formulations, together with several preparation methods, different surfactants (employed in different ratios) have been evaluated. In this work, the triblock copolymer Pluronic, based of poly(ethylene oxide)-b-poly(propylene oxide)-b-poly(ethyleneoxide) (PEO-PPO-PEO), was chosen thanks to its potential capability to increase the brain drug-loaded effect due to its neuroprotective and anti-inflammatory properties described by Serbest et al. [21–23]. In the nanocarrier development stage, several parameters were considered to make the choice of surfactant, including the hydrophilic-lipophilic balance (HLB) value (surfactants with HLB with lower than 9 refers to lipophilic surfactant while surfactants characterized by HLB values higher than 11 refers to hydrophilic ones). In particular, Pluronic F-127 (HLB 22) in mixture with Sorbitan trioleate (Span 85, HLB 1.8) have been employed. Pluronic F-127 has a higher hydrophilic percentage (70%), with more hydrophilic members (chain of PEO) consisting of higher PEO/PPO ratio [24,25]; while the Span 85 is a lipophilic surfactant [26]. In general, highly hydrophilic surfactants are not able to form alone a stabile vesicular system due to their high aqueous solubility, but stable NSVs could be prepared adding the appropriate amount of cholesterol together with lipophilic surfactant such as Span 85 [27]. In particular, F127 has been used to regulate the hydrophobicity of the Span 85/cholesterol and it could be useful to uniformed lateral distribution of the molecules along the bilayers that could allow the membrane integrity of the niosomes [25,28].

Moreover, Pluronic F-127 is also used for its mucoadhesive and penetration enhancer properties [26]. In addition, Span 85 is formed by three chains of oleic acid which could useful to potentially inhibit endothelial cell activation and to reduce expression of inflammatory molecules [29].

In this work, NSVs and VNBs have been characterized in terms of model drug entrapment efficiency, (Calcein and Nile Red, hydrophilic and lipophilic probe respectively) and release capability. Moreover, NSVs and VNBs have been characterized in terms of (a) hydrodynamic diameter, ζ-potential, (b) morphology by TEM analyses, (c) vesicle bilayer fluidity and (d) physical-chemical stability. VNBs have been also characterized in terms of entrapping gas ability and acoustic efficiency. In addition, in order to understand optimal US parameters to obtain *in vitro* stable cavitation, the acoustic pressure effect, induced by the US wavelets, on VNBs fluorescent probes release kinetics was investigated (at different US frequencies. Finally, extracellular field recordings in area CA1-CA3 of the hippocampus have been carried out in order to assure that empty NSVs do not affect synaptic plasticity in term of long-term potentiation (LTP), a molecular mechanism which underlies learning and memory [30].

The obtained results demonstrated NSVs and VNBs as good candidates to improve N2B drug delivery.

2. Materials and methods

2.1. Materials

Pluronic F-127, Sorbitan trioleate (Span 85), Cholesterol (Chol), Bis [N,N−bis(carboxymethyl)aminomethyl]fluorescein (Calcein), 9-(diethylamino)-5H-benzo[R]phenoxazin-5-one) (Nile Red), Diphenylhexatriene (DPH), Pyrene, Sodium 2-(4-(2-hydroxyethyl) piperazin-1-yl (Hepes), Ethanol F.U., Methanol, Chloroform, Tetradecafluorohexane (PFC) were bought from Sigma-Aldrich (Milan, Italy).

2.2. Methods

2.2.1. Preparation of niosomes and nanobubbles

Niosomes (NSVs) were prepared by the thin film layer preparation technique described by Marianecci et al. [31], using several amounts of Pluornic F-127 and Span 85 and Chol (Supplementary Material,

Tables S1 and S2), the chosen formulation is reported in Table 1. The process involves the solubilization of surfactants and/or lipophilic components (DPH/Pyrene/Nile Red) in the organic solvent followed by the solvent evaporation. The dried films were hydrated by Hepes buffer (0.01 M, pH 7.4) or Calcein solution 10^{-2} M (CA). The obtained dispersion was vortexed and then a microtip-sonication (Vibracell-VCX 500, Sonics, Taunton, MA, USA; amplitude 20%, temperature 2 min, 25 °C that increases until up 60 °C during sonication) was employed to obtain unilamellar vesicles. The sonication parameters were analogues with respect to nanobubbles in order to obtain VNBs/NSVs with similar physical-chemical features. Subsequently, the vesicles were extruded at room temperature (RT) by a Lipex ExtruderTM (Vancouver, Canada) equipped with polycarbonate membrane filters. The suspensions were extruded through cellulose filters (Millex1 Syringe Filters, Millipore) of 1.2 μm pore size (2 cycles). By dialysis process, the un loaded CA has been removed. Nanobubbles (VNBs) were prepared following the thin film layer preparation technique, with the same amounts of niosomal components (Table 1) but liquid PFC was added with a syringe to a vesicular dispersion, at RT and subsequently the suspension has been sonicated for 3 min, with an ultrasound generator equipped with a micro-probe operating at 20 kHz, with amplitude of 20% at 25 °C that increases until up 60 °C during sonication (Vibracell- VCX 400-Sonics, USA) following the technique adopted by Hanieh et al., 2022 [18]. Then, the nanobubble dispersion was cooled by thermal shock in melting ice for 10 min. As a final step, the VNBs were extruded at RT through cellulose filters of 0.45 μm (1 cycle) and subsequently by cellulose filters of 0.22 μm pore size (1 cycle), VNBs were immediately collected in a bath ice. VNBs were characterized in terms of acoustic efficiency, entrapment efficiency, release probes capability under US treatment, hydrodynamic diameter, and ζ-potential; the obtained results were compared with those of NSVs.

2.2.2. Dynamic light scattering (DLS)

NSVs and VNBs were characterized in terms of hydrodynamic diameter and ζ-potential. The hydrodynamic diameter and the ζ-potential were characterized by dynamic light scattering (DLS, Malvern Zetasizer Nano ZS90, Malvern Instruments Ltd., Worcestershire, United Kingdom). The instrument measures the mass distribution of particle size as well as the dispersed particle electrophoretic mobility. Reported data represent means of the measurements of ζ-potential (mV) and of the hydrodynamic diameter (nm) for the surfactant vesicles. The polydispersity index (PDI) value was determined as a measurement of the breadth of the size distribution: a PDI value lower than 0.3 indicates that the sample is characterized by homogeneous and monodisperse population.

2.2.2.1. Physicochemical stability over time. Sample hydrodynamic diameter and ζ-potential variations over time were analysed to evaluate physical stability of NSVs and VNBs. The vesicular formulations were stored at 4 or 25 °C for a period of 45 days. Samples from each batch were withdrawn at definite time intervals (1, 15, 30 and 45 days) and the ζ-potential and the mean of hydrodynamic diameter of vesicles were determined as previously described with DLS technique.

2.2.2.2. Physicochemical stability in simulated biological fluid. The stability of empty NSVs was determined after incubation of each sample in Simulated Nasal fluid (SNF) (2.192 g NaCl, 0.145 g CaCl2 and 0.745 g KCl in 250 mL) containing mucin (0.1%, w/v) at 34 °C [32]. After 1, 2, and 3h the mean hydrodynamic diameter, ζ -potential and PDI of the nanoparticle suspensions were measured by DLS. In particular, 0.55 mL of the sample (55%) were added to 0.45 mL of SNF containing mucin (0.1% w/w) (45%) and put into a test tube, magnetic stirring was applied and the temperature was maintained at 34 °C.

Stability studies in artificial Cerebrospinal Fluid (aCSF, pH 7.3) were also carried out on empty NSVs and VNBs preparations. The aCSF composition is reported in Table 2. To evaluate the hydrodynamic diameter, the PDI, and the ζ -potential of the vesicular systems in presence of biological media, the measurements were carried out by DLS at different times (0, 1, 2, and 3h). In particular, 0.55 mL of the sample (55%) were added to 0.45 mL of aCSF (45%) and put into a test tube, a magnetic stirring was applied, and the temperature was maintained at 37 °C [33].

Table 1
Sample composition.

Sample	Span 85 (mM)	F-127 (mM)	Chol (mM)	PFC (mL)
NSVs	10	5	15	–
VNBs	10	5	15	0.5

2.2.3. Transmission electron microscopy (TEM)

The structure of both NSVs and VNBs was visualized by negative staining for transmission electron microscopy (TEM). In brief, the samples were placed on a carbon-coated copper grid (400 mesh; Agar Scientific, UK) and allowed to settle for 1 min before being blotted away with filter paper. A 2% phosphotungstic acid solution (pH 7.2) was added to the grids for 1 min before the solution was blotted away and the grid allowed to dry. Images were recorded at 100 kV by a FEI 208S transmission electron microscope (FEI, Eindhoven, The Netherlands). Adobe Photoshop CS4 software (Adobe Systems, San Jose, CA, USA) was used to optimize image editing.

2.2.4. Fluorescent measurements

2.2.4.1. Bilayer characterization. Fluorometric analysis was carried out to characterize the vesicular bilayer fluidity, preparing the samples with DPH, a lipophilic fluorescent probe (as described in M&M section) used to evaluate the anisotropy value, which is a parameter correlated to rigidity or fluidity of a membrane [34]. DPH fluorescent measurements were performed using a luminescence spectrometer (LS5013, PerkinElmer, Waltham, MA, USA) at room temperature. The excitation and emission wavelengths were 400 and 425 nm, respectively. By employing Equation (2), the fluorescence anisotropy (r) was determined:

$$\text{Fluorescence anisotropy (r)} = \frac{(Ivv \times Ivh) \times G}{(Ivv + 2Ivh) \times G} \quad (2)$$

where I_{vv}, I_{vh}, I_{hv}, and I_{hh} are fluorescent intensities, subscript v (vertical) and h (horizontal) represent the orientation of polarized light, and $G = I_{hv}/I_{hh}$ factor is the ratio of sensitivity of the detection system for vertically and horizontally polarized light.

2.2.5. In vitro release studies of NSVs

In vitro drug release experiments were carried out putting the CA/NR loaded sample in a dialysis bag (molecular weight cut-off: 8000 by Spectra/Por®). The dialysis bag was immersed in the release medium (Hepes Buffer 10 mM, pH 7.4 or aCSF, pH 7.3) at 37 °C and gently magnetically stirred during the experiment. The CA/NR concentration in the acceptor medium was detected at different times points (0, 1, 2, 3, 4, 5, 6, 7, 8 and 24h), respectively by a fluorimeter (LS5013, PerkinElmer, Waltham, MA, USA) or UV spectrophotometer (Lambda 25,

Table 2
Artificial cerebrospinal fluid (aCSF): chemical composition.

Reagent	Concentration (mM)
NaCl	124
KCl	3
$NaHCO_3$	26
NaH_2PO_4	1.25
$MgCl_2$	1
$CaCl_2$	2

PerkinElmer, Waltham, MA, USA). In order to perform quantification analysis, 1 mL of external medium was withdrawn and immediately analysed and then re-inserted back. The % of released probe was calculated considering the ratio between the Fluorescence (CA) or the absorbance (NR), detected at specific time point, over the Fluorescence (CA) or the absorbance (NR) maximum of the samples, both measures are made at the same dilution. The collected data represent the mean values over three repeated independent experiments, and errors are the standard deviation.

2.2.6. Acoustic attenuation and ultrasound in vitro characterization

2.2.6.1. Pulse-echo technique. An ultrasonic pulse-echo technique was used to determine the VNBs scattering efficiency over time. The acoustic attenuation was measured over the −6 dB bandwidth of the ultrasonic transducer through the amplitude and frequency analysis of a short ultrasound pulse crossing twice a test-cell containing a VNBs suspension. The obtained spectrum of the back-scattered signal provides information on the acoustic efficiency of the VNBs over that bandwidth, and on the ultrasonic frequency at which the acoustic wave is mostly attenuated by the VNBs. The buffer solution in the test-cell has been measured as a reference medium [18].

2.2.6.2. Ultrasound in vitro characterization. US *in vitro* treatment was performed using Sonowell®, an integrated automated instrument (Inno-Sol srl, Rome, Italy). The instrument is designed for the use on commercially available wells plates and ensures the necessary control conditions of temperature by partially immersing the wells plate, bottom and side-walls, in a thermostated water bath tank. The configuration of the used instrument comprises 4 independent parallel channels generator/amplifier (20W max power) delivering frequencies in the range 0.5–5.0 MHz, running four different single element "flat" transducers, 12-mm diameter active membrane, with frequencies 0.65, 1.0, 2.4, and 4.5 MHz that can hold an acoustic intensity emission per frequency up to 6 W/cm^2 (CW 60 s).

The instrument is run via the software, SonoWell Soft© installed on a laptop controlling the instrument the topology of the motorized movement of the plate-well on the transducers, as well as handling time and acoustic intensity delivery on each well independently (frequency, power, duty cycle, repetition frequency, well time, etc.) via a graphical interface.

Transducers are positioned below the plate, immersed in the distilled water tank and positioned in an *ad-hoc* designed holder, which keeps them at constant temperature by means of an independent cooling circuit. The holder positions each transducer at a different fixed distance from the plate bottom, depending on the frequency, in such a way that they share the same near and far field plane. The use of a collimator plate inserted between the transducers and the plate-well bottom ensures that no diverging US wavelet is invading, from the bottom, the wells neighbouring the sonicated one. Since acoustic intensity used was rather high, it has been necessary to use the Block-US polymer (Inno-Sol srl, Rome, Italy), to dampen conversion modes acoustic transverse invasion of nearby wells, Fig. 1B (and Supplementary material Fig. S1). Briefly, this patented technology minimizes the problems arising from the induced "leakage" shear waves orthogonal to the main direction of propagation within the well, including the conversion modes waves generated by the interaction of the US wavelets with the polystyrene bottom lamina of the well plate [35–38]. The rationale behind and the use of this technology and its implementation in the experiments is detailed in the Supplementary Material.

Great care was taken in entirely filling the well volume ensuring that no air was entrapped upon positioning the well plate cover, securing the wells top edges with a silicon grease film (Molykote 111 Compound, Dow Corning, Michigan, USA) which perfectly adheres to the plate cover. This set-up avoids risks of contaminating wells via aerosol creation and travelling. A mate of Aptflex F28 (frequencies >1.0 MHz) or F48 (frequencies ≤ 1.0 MHz) (Precision Acoustics, UK) was positioned on top of the cover to adsorb US waves and avoid reflections at the air interface (Fig. 1D).

Experiments were always conducted allowing a pre-equilibration of the plate of at least 5 min with water thermostated at 37 °C.

Acoustic intensity calibrations were performed using an immersion needle 0.5 mm diameter hydrophone needle/preamplifier (Precision Acoustics, UK) interfaced with a portable scope meter Fluke 125 (Wilmington, NC) for detection of the wave signal.

2.2.6.2.1. US in vitro protocol. To characterize how the US affected the cavitation of VNBs the kinetics of drug release was monitored at 37 °C, samples (total volume were 1 mL with 55% of VNBs loaded CA, hydrophilic model drug, and 45% of Hepes buffer) were placed in dialysis bags, cellulose membrane Spectra/Por® molecular weight cut-off 8000 and 5.5 cm^2 diffusing area. Dialysis started by inserting the bags in 12 well plates against 5.0 mL Hepes buffer as external medium.

To establish the US induced effect several experiments at increasing acoustic pressures were applied to the wells containing the drug loaded VNBs, until an effect on the release kinetic was clearly and reproducibly monitored. The optimization of relevant sonication parameters was achieved with an array of experiments on 12-well plates (an example is shown in Supplementary Material Fig.S5). The parameters explored were the Sonication Frequency (SF) [650 kHz, 1.0 MHz, 2.4 MHz and

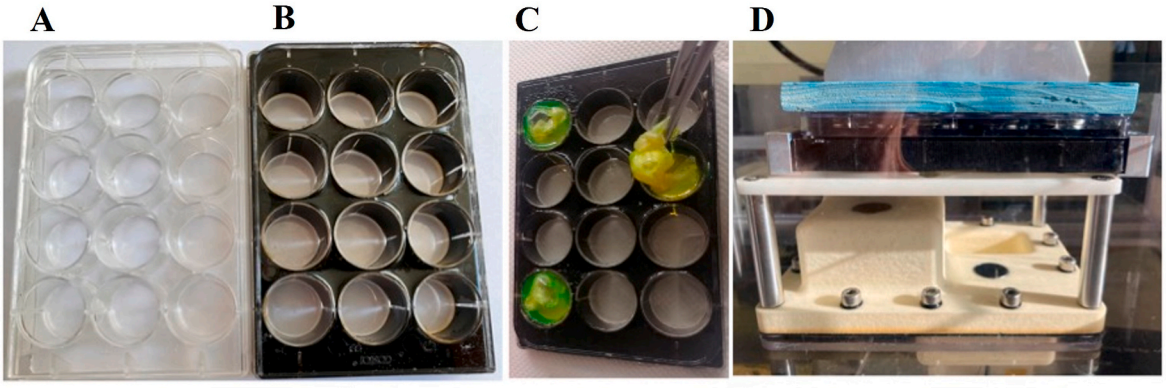

Fig. 1. Example of preparation of the 12 wells-plate with the Block-US polymer. (A) The original Corning Costar plate; (B) Same after preparing the plate inserting Block-US polymer; (C) A typical introduction of the VNBs samples inserted in the dialysis membranes secured with mini-knots and encased within the well; (D) The plate thus prepared with the cover positioned, as explained in the methods section below, and inserted in the SonoWell plateholder positioned on the 4 transducers, in cyan the F48 adsorber mate on the cover, adhesion ensured with few drops of water forming a film. (For interpretation of the references to colour in this figure legend, the reader is referred to the Web version of this article.)

4.5 MHz], the Sonication Time (ST) [30, 60 and 180s], and the levels of acoustic pressure (AP) [range 40 kPa - 2.0 MPa], Table 3. The other relevant sonication parameters were kept constant: Duty Cycle (DC) 40%, Sonication Burst (T_{on}) 10.0 ms, Pulse Repetition Frequency (PRF) 40Hz; further experimental details in Supplementary Material.

Once established the relevant parameters of SF, AP and ST the design of the experiment positioned the samples only in wells A2, C1 and C4 of the plate (Fig. 1C), while the non-sonicated controls were kept in a thermostated plate not loaded in the SonoWell instrument.

The sonication protocol chosen for all the remaining experiments was performed at 650 kHz and 37 °C for 180 s using a single 12-wells plate in which a dialysis bag was positioned to simulate the model drug release. The experiments were carried out in triplicates on different wells to estimate mean value and its standard error.

At pre-determined time intervals (pre-US 5 min, post-US immediately, 1h, 3h, 6h and after 24 h), aliquots from the external medium were taken out and analysed with a spectrometer (LS5013, PerkinElmer, Waltham, MA, USA) using CA parameters, excitation and emission wavelength 492 nm and 520 nm respectively. Similar to the procedure adopted for CA, to mimic an hydrophobic model drug, NR has been used and the experiment was carried out in the same conditions described for CA. At pre-determined time intervals aliquots from external medium were analysed using a UV–vis spectrophotometer (Lambda 25, PerkinElmer, Waltham, MA, USA). NR samples analyses were carried out in scan mode (700–200 nm) following the NR characteristic peak at 570 nm, by means of a spectrophotometer equipped by 1.0 cm path-length quartz cells. The "% Release" was calculated considering the ratio between the Fluorescence (CA) or the absorbance (NR), detected at specific time point, over the Fluorescence (CA) or the absorbance (NR) maximum of the samples.

After US treatment, formulations were characterized by DLS measurement as reported in paragraph 3.2 and by Anisotropy analyses as reported in section 3.4.1.

2.2.7. Electrophysiology

This study was carried out in accordance with the recommendations of international guidelines on the ethical use of animals from the European Communities Council Directive (2010/64/EU).

2.2.7.1. Slice preparation. C57BL6/J mice (30–40 days old, male and female) were killed by decapitation. The brain was rapidly removed from the skull and parasagittal hippocampal slices (350 μm) were cut with a vibratome (VT 1200S, Leica) in cold (0 °C) artificial cerebrospinal fluid (aCSF) containing (in mM): NaCl (124); KCl (3); MgSO4 (1); CaCl2 (2); NaH_2PO_4 (1.25); $NaHCO_3$ (26); glucose (10); saturated with 95% O_2, 5% CO_2 (pH 7.4), and left to recover for 1 h in aCSF at 33.5 °C.

2.2.7.2. Extracellular recordings. Extracellular field recordings were performed in region CA1-CA3 of the hippocampus. Field excitatory postsynaptic potential (fEPSP) was elicited with a stimulating electrode placed in CA3 in the Schaffer collateral pathway and recorded with a glass electrode placed in CA1. Paired pulse ratio (PPR) was assessed at inter-stimulus intervals from 50 to 500 ms and was calculated as ratio of the second fEPSP amplitude/first fEPSP amplitude. In synaptic plasticity experiments, a baseline (20 min) was recorded before the induction of Long-Term Potentiation (LTP) using a theta-burst stimulation protocol consisting of four pulses at 100 Hz, with the bursts repeated at 5 Hz and each tetanus including three 10-burst trains separated by 15 s. Then responses were recorded for 1 h after tetanization and measured as fEPSP amplitude normalized on baseline. Before recordings, some slices were incubated with formulations (NSVs) for 30 min [39]. The dilutions of NSVs (30 and 100 μM) were made considering the concentration of Pluronic F-127 in a total volume of 10 mL of aCSF saturated with 95% O_2 and 5% CO_2. Results are reported as mean ± S.E.M.

2.2.8. Statistical analysis

For the statistical analysis of NSVs or VNBs characterization studies, two-way ANOVA was performed. Multiple comparisons were performed according to Tukey's test for **ζ** -potential, hydrodynamic diameter, and polydispersity index (PDI), respectively. Any p-value <0.05 was considered statistically significant. A p-value of less than 0.05 ($^*p < 0.05$) was considered significant. For ultrasound experiments data shown are the mean ± S.E.M of three independent assays. Statistical differences between groups were analysed using Student's *t*-test. The difference was considered statistically significant at p value of less than 0.05. For electrophysiology experiments the statistical significance was evaluated by Student's t-test between 50 and 60 min following delivery of conditioning trains. Statistical significance was set at $p < 0.05$ and n was the number of slices.

2.3. Results and discussion

2.3.1. Characterization of niosomes and nanobubbles

Several formulations of NSVs and VNBs prepared with different techniques were analysed in terms of hydrodynamic diameter and ζ-potential and the selected formulations have been reported in Table 1. Niosomes NSVs were prepared with thin layer evaporation technique [31], while VNBs followed the same protocol reported in previous

Table 3
Sonication protocols acoustic parameters generating High and Low Acoustic Pressure.

Experimental Acoustic Pressure	f **(MHz)**	I_{spta} **(W/cm²)**	kPa (p^-)	Mechanical Index $MI^* = p^- / \sqrt{f}$
High	0.65	4.21	450	0.56
High	1.0	3.72	811	0.81
High	2.4	3.10	1265	0.82
High	4.5	2.11	1930	0.91
Low	0.65	0.95	40	0.05
Low	1.0	0.46	40	0.04
Low	2.4	0.23	40	0.03
Low	4.5	0.11	40	0.02

$^*p^-$ = negative pressure peak; f = US frequency.

Table 4
Size (DLS), charge (ζ-potential) and bilayer characterization in terms of anisotropy. Listed values are determined as the mean ± standard deviation of n = 3 NSVs and n = 3 VNBs sample measurements.

Sample	Hydrodynamic diameter (nm) ± SD	ζ-potential (mV) ± SD	PDI ± SD	Anisotropy	Acoustic attenuation (dB/cm)
NSVs	163.4 ± 0.097	−8.45 ± 0.191	0.253 ± 0.001	0.15	2.1
VNBs	289.2 ± 12.38	−27.1 ± 4.55	0.281 ± 0.041	0.23	14.3

studies [18]. Both samples have been characterized in terms of hydrodynamic diameter, ζ-potential, PDI, anisotropy, and VNBs also in terms of acoustic attenuation. The obtained results are reported in Table 4. DLS analysis shows a hydrodynamic diameter increase of VNBs (289.2 nm) with respect to NSVs (163.4 nm) and this data suggest the inclusion of gas into the vesicles. This result is supported by both anisotropy and ultrasonic attenuation measurements. In fact, in Table 4 it is possible to observe that the anisotropy value (parameter related to bilayer rigidity/fluidity, higher anisotropy values correspond to higher bilayer rigidity) increases in VNBs samples with respect to NSVs, probably due to the gas interaction with the bilayer vesicles [40]. Furthermore, the acoustic efficiency of the empty and loaded vesicles (measured by a pulse-echo technique) confirms the gas internalization highlighted by the significant higher acoustic attenuation of VNBs with respect to NSVs (14.3 dB/cm and 2.1 dB/cm respectively). NSVs exhibit a (low) acoustic attenuation solely due to the acoustic impedance mismatch between the NSVs outer shell and the buffer solution leading to a reflection of a small fraction of the incident acoustic energy.

Tacking in to account the ζ-potential values reported in Table 4 it is possible to observe significant differences between NSVs and VNBs. In particular, the samples prepared in presence of gas, are characterized by ζ-potential values more negative in comparison with NSVs. Probably, the gas internalization affects the Pluronic distribution within the vesicles bilayer, leading to an increase of the Pluronic charged moiety towards the external surface of the VNBs (Fig. 2) [40]. Consequently, the ζ-potential values decrease from −8.45 to −27.1 mV also affecting vesicle stability as discussed below. Finally, it is possible to underline that, for both formulations, the collected size range is suitable for the N2B delivery [41] and that both formulations are characterized by an appropriate PDI value (below 0.3) that represent a monodisperse sample [42]. (FDA's "Guidance for Industry" concerning liposome drug products emphasizes the importance of size and size distribution as "critical quality attributes (CQAs)", as well as essential components of stability studies of these products) [42].

2.3.1.1. Morphological characterization. Fig. 3 shows the transmission electron micrographs of the empty NSVs and corresponding VNBs after PFC filling. Both samples showed an almost spherical shape. A thin shell surrounding the core of vesicles suggested an envelope with likely unilamellar structure. Surface morphology did not appear significatively different between empty, and gas filled vesicles. Although subject to artefacts introduced by sample preparation due to drying steps, TEM images indicated that the vesicle sizes are in agreement with those measured by DLS. PFC filled nanobubbles appeared larger compared to empty niosomes due to gas internalization.

2.3.2. Stability studies

2.3.2.1. Physical stability over time. The sample stability over time is fundamental for the development of a commercial product to be employed in diagnostics or theranostic field. At this purpose, physical stability (Figs. 4 and 5) over time for both samples (NSVs and VNBs), was carried out detecting hydrodynamic diameter, ζ-potential and acoustic efficiency variation until up to 45 days at two different storage temperatures, 4 °C and room temperature (RT). By the results obtained it is possible to conclude that NSVs at 4 °C storage temperature was stable in terms of size and ζ-potential while at RT its hydrodynamic diameter significatively increased during the experiment. Probably, the dispersed vesicle stability was affected by temperature and ζ-potential values. In fact, the colloidal dimensions at 4 °C were maintained because of the reduced collision events between dispersed vesicles. At RT, the collision phenomena are more significant, and the very low ζ-potential value doesn't preserve the sample by coalescence phenomena with consequent size increasing [43–46]. On the other hand, VNBs are stable at both temperature in terms of hydrodynamic diameter until 45 days, probably thanks to ζ-potential value (≈−30 mV) [47] that assures a good colloidal stability due to the presence of electrostatic repulsion force that prevent aggregation phenomena. The vesicle stability could be also influenced by bilayer rigidity. A slight increase of anisotropy values was observed for VNBs with respect to NSVs indicating an increase in the bilayer rigidity that could enhance the nanocarrier stability [45,48].

Fig. 6 reports VNBs stability over a period of 45 days measured in terms of acoustic attenuation probed at 14 MHz with a pulse-echo technique. Acoustic attenuation decreases with time with a slower decrease for VNBs stored at 4 °C than for those stored at 25 °C. After 45 days, VNBs stored at 4 °C show an attenuation well above 7 dB/cm, a value comparable to that of some commercially available ultrasound contrast agents (UCA) such as Sonovue® or Levovist® [49,50] that, moreover, being unstable they must be reconstituted at the time of application.

2.3.2.2. Stability in simulated biological fluid. Intranasal administration is an attractive possibility to enhance the biodistribution and localization of the entrapped drug inside the nanocarriers to CNS. To evaluate the effect of physiological media on the nanocarrier integrity, *in vitro* stability studies in simulated nasal fluid (SNF) were carried out. In more detail, stability studies were carried out in SNF containing mucin (0.1% w/v) at 34 °C evaluating the vesicle size variations by DLS for 3h as described before (Section 2). By the obtained results reported in Fig. 7, it is possible to observe only a slight increase of the nanocarrier dimensions during the experiment that could be explained by a partial coating of the vesicles surface by SNF components. Despite this, it is possible to conclude that SNF doesn't affect the vesicles' integrity [51].

The stability of NSVs was also studied in artificial cerebrospinal fluid (aCSF, Fig. 7) to mimic the effect of the media on the vesicle stability after intranasal administration. The experiments were carried out at 37 °C evaluating the vesicle size by DLS for 3h as described before

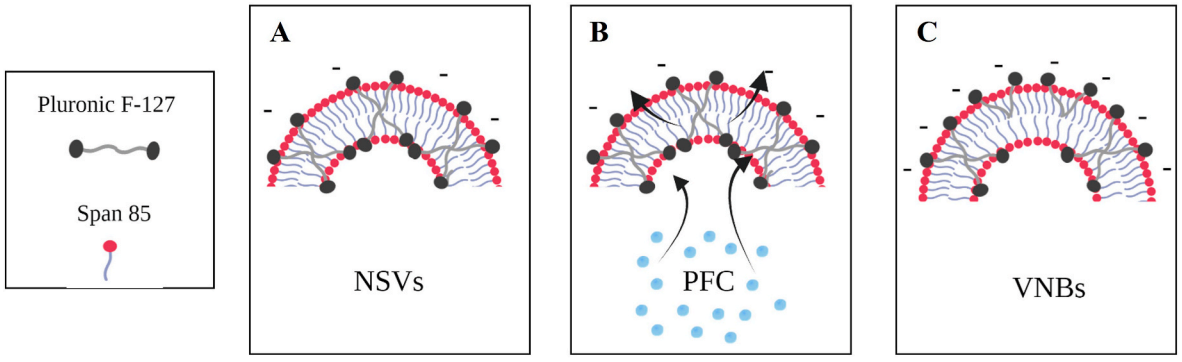

Fig. 2. Schematic cartoon of supposed gas-vesicle interaction: effect on the surface charge: (A) Niosomes NSVs; (B) Supposed interaction of PFC with surfactant bilayer components; (C) VNBs results.

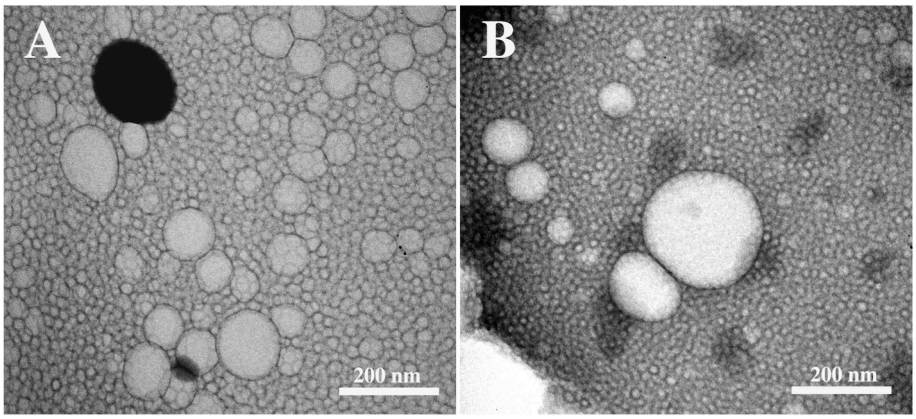

Fig. 3. Electron micrographs: (A) niosomes and (B) nanobubbles visualized by negative staining.

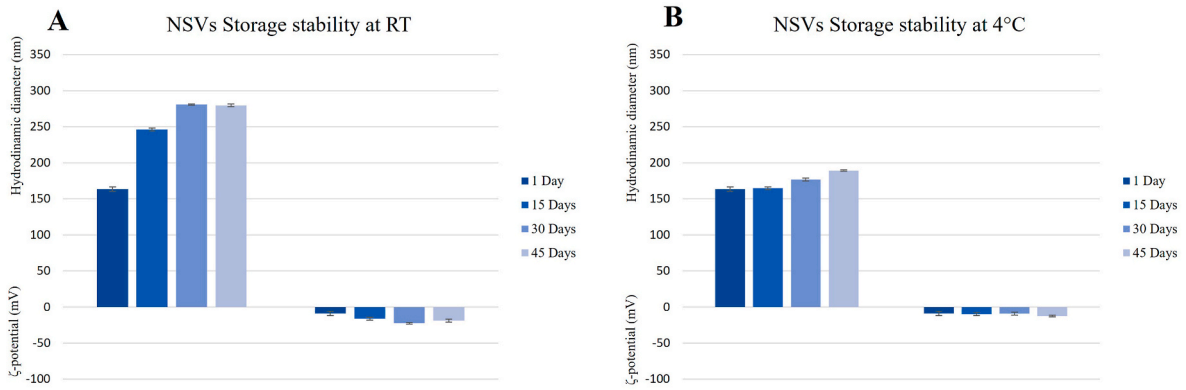

Fig. 4. Physicochemical stability over time: result of investigation on physicochemical stability of empty niosomes (NSVs) in terms of hydrodynamic diameter and ζ-potential until up to 45 days, (A) at room temperature (RT); (B) at 4 °C.

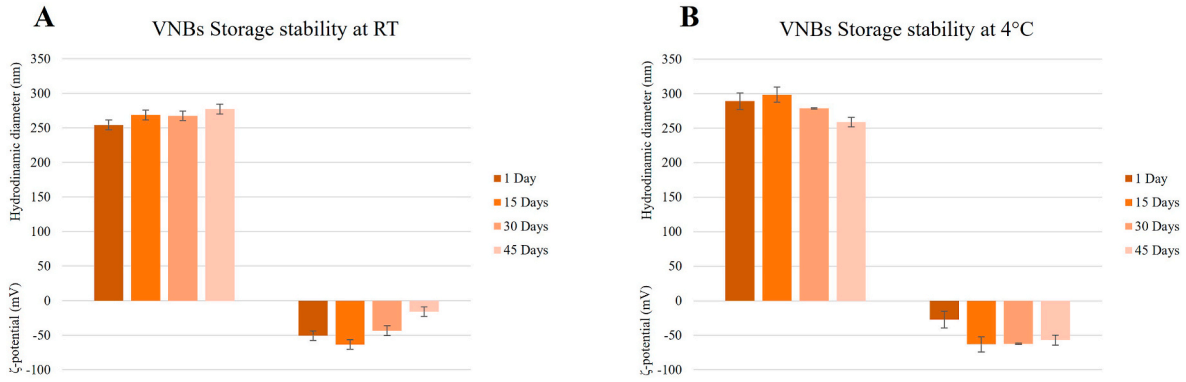

Fig. 5. Physicochemical stability over time: Result of investigation on physicochemical stability of empty nanobubbles (VNBs) in terms of hydrodynamic diameter and ζ-potential until up to 45 days, (A) at room temperature (RT); (B) at 4 °C.

(Section 2) [26]. During the experiment, no significant changes in hydrodynamic diameter were observed therefore it is possible to conclude that aCSF media doesn't affect the vesicles integrity [52].

2.3.3. *In vitro release capability by NSVs*

In vitro release studies of CA-NSVs and NR-NSVs in Hepes and aCSF have been carried out to study the effect of different media on the release capability of the vesicles and the data obtained are shown in Fig. 8. The total amount of released CA of NSVs is around 100% at 24 h in Hepes buffer and a similar released amount of CA in aCSF has been shown. The same results are obtained by NR release study. In fact, the NR percent released is the same in both media. The lower amount of NR released with respect to CA, probably is related to its lipophilic nature [53]. In conclusion, it is possible to conclude that the aCSF media doesn't influence the release capability of the nanocarriers.

2.3.4. *Acoustic and ultrasound results*

2.3.4.1. US treatment for VNBs stable cavitation. A set of US experiments performed on the drug CA loaded VNBs, were designed to determine US parameters generating the minimum acoustic pressure able to induce a stable cavitation effect. In fact, cavitation affecting VNBs' structure in a

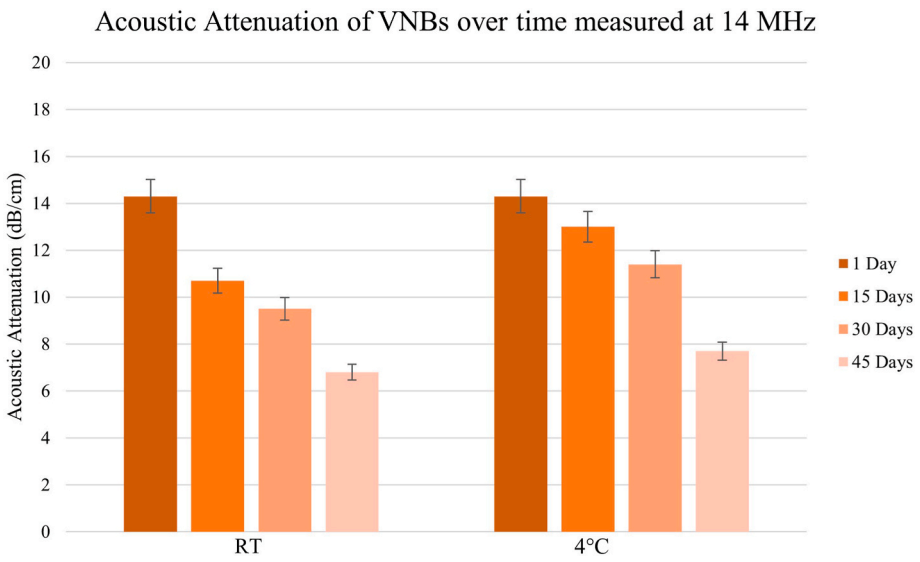

Fig. 6. Acoustic attenuation over time at 14 MHz: Results of acoustic attenuation stability over time of VNBs at room temperature (RT) and at 4 °C measured at 14 MHz.

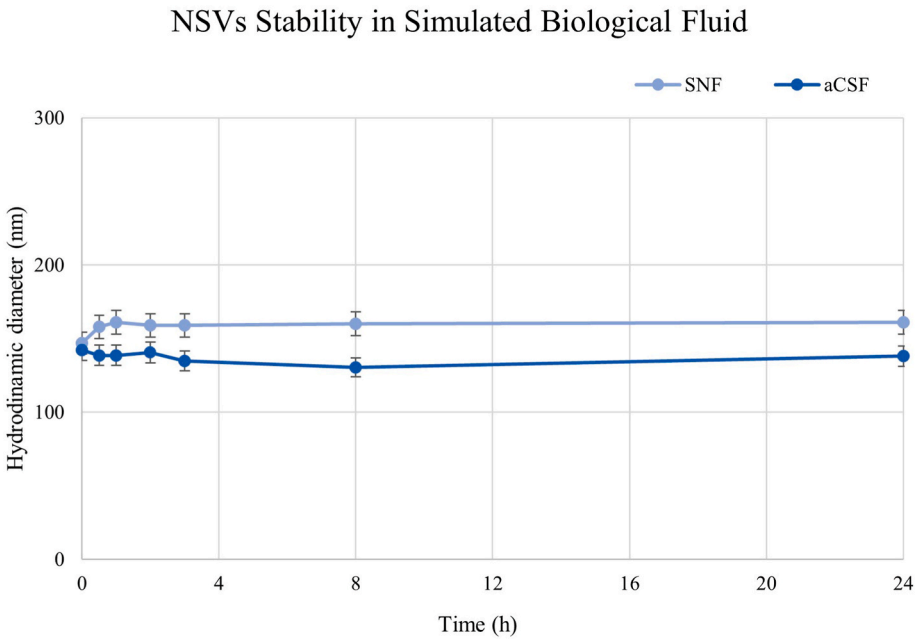

Fig. 7. Stability studies in biological fluids: Stability studies in the presence of SNF and mucin (0.1% w/w) and aCSF, following variation of hydrodynamic diameter values of empty niosomes (NSVs).

reversible manner, would enhance the amount of the fluorescent drug released, whose monitoring acts as marker of success. The goal was to establish an appropriate combination set of US parameters able to induce stable cavitation while still keeping the index of safety, "mechanical index" (MI), below its safety threshold limit, MI value < 0.7, as established by the British Medical Ultrasound Society [54], in order to avoid tissue damage or induced bleeding. This goal is two-fold important: for safety reason in *in-vivo* experiments, and for demonstrating that our VNBs formulation of the size ≈300 nm can be induced to stable cavitation. The latter is a task relevant for performing future *in vivo* experiments since VNBs should co-adjuvate the delivery of drug loaded NSVs.

To this purpose several experiments were performed at 4 different frequencies, namely 0.65, 1.0, 2.4 and 4.5 MHz, and electric power was varied to increase the acoustic pressure until a clear effect on the VNBs drug release kinetic was recorded, the corresponding acoustic pressure was fixed as the High value in Table 3. A clear effect increasing the rate of drug release from VNBs was visible for 0.65 MHz as well as 1.0 MHz, while no marked effect was visualized even at the highest acoustic pressures of ~ 1.2 and ~ 1.9 MPa respectively reached with 2.4 and 4.5 MHz. Hence a time course release followed for over 30 h was monitored only for the 0.65 and 1.0 MHz frequencies. In Table 5 are reported the estimates of the kinetic constant for the drug release of the CA loaded VNBs in control and US sonicated wells obtained by fitting the time-course acquired data (Supplementary material Fig. S6).

The speed of drug release is thus increased of 2.1-fold for the sonication conditions at 0.65 MHz while the increase is of ~ 1.5-fold at 1.0 MHz.

Tests were also performed to verify a) that integrity of the dialysis membrane was not affected by the acoustic pressure exposure and b)

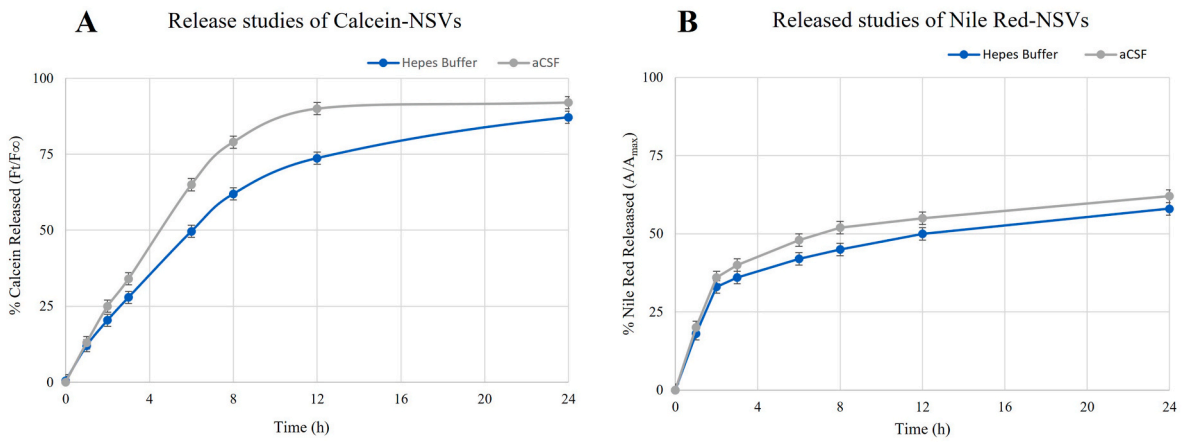

Fig. 8. Release studies: (A) Calcein and (B) Nile Red release profile of NSVs until up 24h. Data were obtained ad the mean of three independent experiments. (For interpretation of the references to colour in this figure legend, the reader is referred to the Web version of this article.)

Table 5
Data on the fluorescent probe release kinetic constant were obtained by measurements of the CA concentration released into the buffer at several timepoints and fitting the triplicate data with an equation $y = A\ (1 - e^{-Bt})$. The resulting values of **B** for 0.65 and 1.0 MHz are shown below.

Condition	Kinetic constant at 0.65 MHz [h^{-1}] ± SD	Kinetic constant at 1.0 MHz [h^{-1}] ± SD
US	0.34 ± 0.09	0.28 ± 0.09
Ctrl	0.16 ± 0.02	0.19 ± 0.04

that the VNBs were not destroyed during the high intensity sonication. In fact, the Hydrodynamic Diameter evaluated for the VNBs after being exposed to cavitation (Supplementary Material Table S4) were roughly 20% increased for the 0.65 MHz, while were about 4% decreased in the 1.0 MHz US sonication. In both cases considering that these values are averages of a population distribution, they are not large enough to be considered significative.

The lower frequency of 0.65 MHz was then chosen to continue the characterization as the most suitable since its MI value of 0.56 was well below the threshold limit of 0.7, Table 3, and its increase in the kinetic of drug release is larger than that of 1.0 MHz.

The evidence that the lower US frequency, 0.65 MHz, results into a CA release at about 450 kPa of peak negative pressure, and requires slightly more that 800 kPa for the 1.0 MHz is in agreement with the theoretical studies by Apfel & Holland (1991) [55] and Ahmadi & McLoghlin (2013) [56], where they show that it is possible to semi-quantitatively describe with an analytical function the relationship between the bubble behaviour and the acoustic wave frequency *(SF)* and that the behaviour can define a cavitation threshold which depends on the negative peak of the acoustic pressure and the diameter of the bubble. The former produced a simplified analytical model applied to SF of 1 MHz or higher, while the latter bridged the gap left for the frequencies lower than 1 MHz, extending the equations of the analytical model and applying them for SF in the range 20 kHz up to the MHz range.

Taking into account both the studies, semi-quantitatively the cavitation threshold for a nanobubble of approximately ≈300 nm is expected >400 kPa at 650 MHz, while for 1.0 MHz is expected >700 kPa.

The fact that we don't have evidence of drug release at the higher SFs might be interpreted as lack of stable cavitation, having not reached the minimum threshold of acoustic pressure necessary for the bubble to resonate in the acoustic field.

2.3.5. Electrophysiological results

2.3.5.1. The effect of NSVs on paired pulse facilitation and long-term potentiation. In the view to use this model of NSVs to delivery drugs to the brain for the treatment of neurodegenerative disorders, electrophysiological recordings on *ex vivo* hippocampal slices were performed to evaluate the effect of NSVs on synaptic transmission and plasticity (Fig. 9A Schematic representation of hippocampal slices incubation process before electrophysiological recordings). In particular, it was carried out extracellular field recordings in area CA1-CA3 of hippocampus to assess the PPR and LTP of pre-treated slices with NSVs for 30 min. Dilutions of NSVs (30 and 100 μM) tested were made considering the concentration of Pluronic F-127, based on results showed by Pluronic P-188 which has similar molecular structure [57], and also considering the relative concentration of Span 85 which is cytotoxic at high dose [58]. The PPR obtained from slices pre-treated with NSVs at both concentrations tested (30 and 100 μM) did not show any difference compared to control, in fact data indicated that, at all interpulse intervals, PPR was indistinguishable between groups ($p > 0.05$; Fig. 9B). To provide evidence that NSVs do not affect synaptic plasticity, LTP experiments were performed from slices pre-treated with different concentrations. The magnitude of potentiation observed in slices pre-treated with NSVs (30 μM: 150.82 ± 3.04; 100 μM: 145.63 ± 3.18) was comparable to the control slices group (148.29 ± 7.03) ($p > 0.05$, Fig. 9C and D).

3. Conclusion

In this work new NSVs (for drug delivery) and VNBs (potentially able to increase the permeability to the brain of NSVs) based on Pluronic F-127, Span 85 and cholesterol were designed, prepared, and deeply characterised. NSVs and VNBs hydrodynamic diameters were suitable for the supposed administration route and both nanocarriers were resistant and stable in artificial biological fluids (aCSF and SNF) [41]. In addition, both formulations have been evaluated in terms of storage stability time at two temperatures (4 °C and RT) and NSVs were stable until up to 45 days at 4 °C, while VBNs at both temperatures of the experiments. Moreover, VBNs were characterised by a significant acoustic attenuation (14.3 dB/cm) and PFC entrapment efficiency resulting in being able to respond to an US field.

In fact, an *in vitro* US treatment was performed with suitable parameters to induce stable cavitation, as evidenced by the kinetic release increase of a fluorescent probe loaded inside the VNBs, and the result was achieved without affecting the structure of VNBs since the hydrodynamic diameter does not undergo significant changes after US field exposure. The increased release kinetic was obtained at 0.65 MHz and

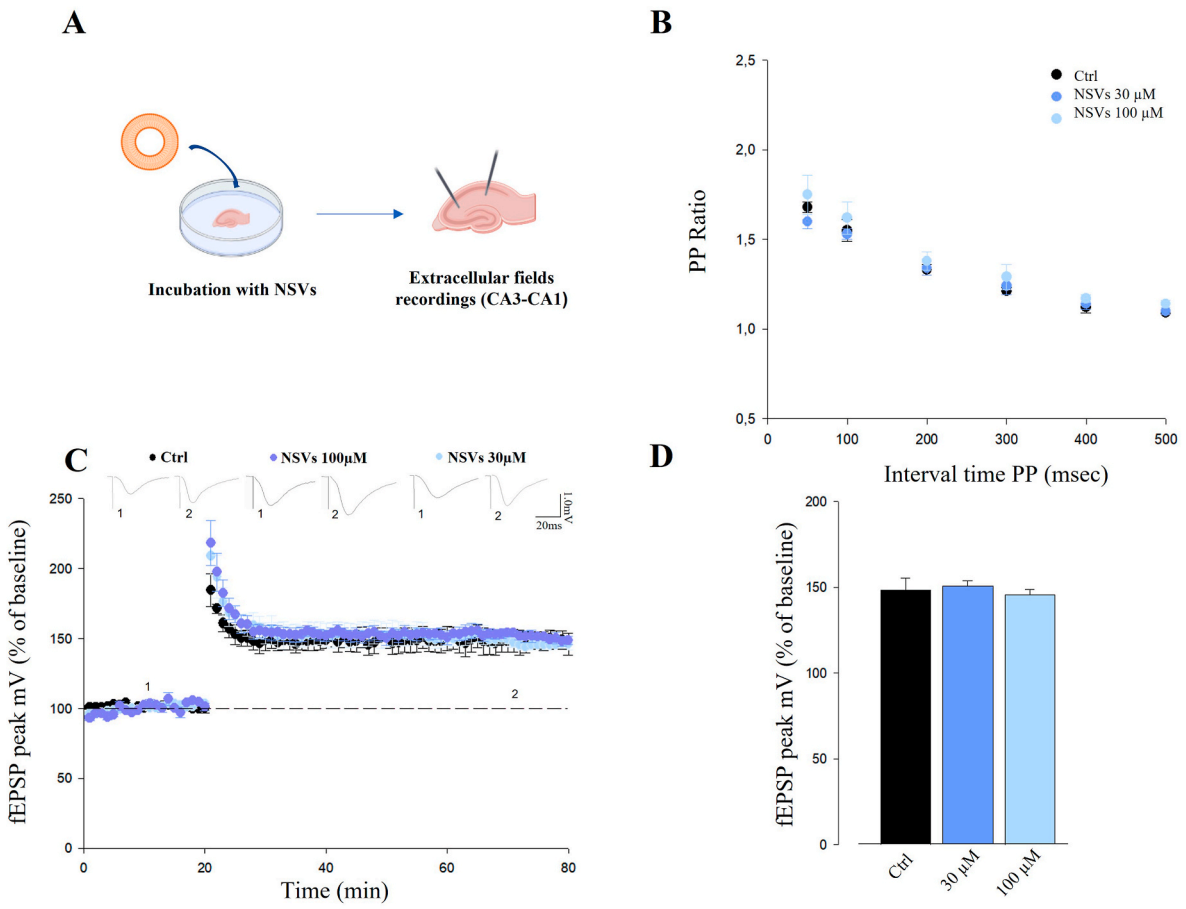

Fig. 9. NSVs do not affect hippocampal synaptic plasticity: Data are presented as mean ± SEM. (A) Schematic representation of incubation process of hippocampal slices; (B) PPR induced by pairs of stimulation delivered at several interstimulus intervals (50, 100, 200, 300, 500 ms); (C) Above representative traces for vehicle and both conditions (30 and 100 µM) are shown; below summary graph of the averaged time course of LTP (Vehicle, n = 5; NSVs 30 µM, n = 5; NSVs 100 µM, n = 5) induced by theta-burst stimulation. (D) Histograms illustrating the magnitude of LTP (% of baseline) in the three experimental conditions.

had an MI = 0.56 which is well suitable for *in vivo* studies.

In the light of functional results, in which NSVs do not induce any variation in synaptic transmission and plasticity, this kind of NSVs model could be used to deliver drugs to the brain for the treatment of neurodegenerative disorders.

Author contributions

N.M.: Conceptualization, Methodology, Validation, Investigation, Data curation, Writing - Original Draft, Writing - Review & Editing, Visualization.

D.M.: Methodology, Validation, Writing - Original Draft, Writing - Review & Editing.

A.B.: Conceptualization, Investigation, Writing - Original Draft, Writing - Review & Editing.

G.B.: Conceptualization, Validation, Investigation, Writing - Original Draft, Writing - Review & Editing, Supervision.

MG.A.: Investigation, Data Curation, Writing - Original Draft, Writing - Review & Editing.

F.R.: Conceptualization, Validation, Investigation, Data curation, Data curation, Writing - Original Draft, Writing - Review & Editing, Visualization, Supervision.

C.M.: Data Curation, Writing - Original Draft, Writing - Review & Editing, Supervision.

M.C.: Data Curation, Writing - Original Draft, Writing - Review & Editing, Supervision.

R.N.: Data Curation, Writing - Original Draft, Writing - Review & Editing, Supervision.

Declaration of competing interest

The authors declare that they have no known competing financial interests or personal relationships that could have appeared to influence the work reported in this paper.

This work has not been published previously, it is not under consideration for publication elsewhere, its publication is approved by all authors and tacitly or explicitly by the responsible authorities where the work was carried out, and that, if accepted, it will not be published elsewhere in the same form, in English or in any other language, including electronically without the written consent of the copyright-holder.

Data availability

No data was used for the research described in the article.

Appendix A. Supplementary data

Supplementary data to this article can be found online at https://doi.org/10.1016/j.jddst.2023.104977.

References

[1] A. Misra, S. Ganesh, A. Shahiwala, S.P. Shah, Drug delivery to the central nervous system: a review, J. Pharm. Pharmaceut. Sci. 6 (2003) 252–273.

[2] S. Bozdağ Pehlivan, Nanotechnology-based drug delivery systems for targeting, imaging and diagnosis of neurodegenerative diseases, Pharm. Res. (N. Y.) 30 (2013) 2499–2511, https://doi.org/10.1007/s11095-013-1156-7.
[3] N.J. Abbott, Blood–brain barrier structure and function and the challenges for CNS drug delivery, J. Inherit. Metab. Dis. 36 (2013) 437–449, https://doi.org/10.1007/s10545-013-9608-0.
[4] D. Furtado, M. Björnmalm, S. Ayton, A.I. Bush, K. Kempe, F. Caruso, Overcoming the blood–brain barrier: the role of nanomaterials in treating neurological diseases, Adv. Mater. 30 (2018) 1801362, https://doi.org/10.1002/adma.201801362.
[5] M.M. Patel, B.M. Patel, Crossing the blood-brain barrier: recent advances in drug delivery to the brain, CNS Drugs 31 (2017) 109–133, https://doi.org/10.1007/s40263-016-0405-9.
[6] X.-Q. Zhang, L. Xu, S.-Y. Yang, L.-B. Hu, F.-Y. Dong, B.-G. Sun, H.-W. Shen, Reduced synaptic transmission and intrinsic excitability of a subtype of pyramidal neurons in the medial prefrontal cortex in a mouse model of Alzheimer's disease, JAD 84 (2021) 129–140, https://doi.org/10.3233/JAD-210585.
[7] L.-A. Keller, O. Merkel, A. Popp, Intranasal drug delivery: opportunities and toxicologic challenges during drug development, Drug Deliv. and Transl. Res. 12 (2022) 735–757, https://doi.org/10.1007/s13346-020-00891-5.
[8] P.C. Pires, A.O. Santos, Nanosystems in nose-to-brain drug delivery: a review of non-clinical brain targeting studies, J. Contr. Release 270 (2018) 89–100, https://doi.org/10.1016/j.jconrel.2017.11.047.
[9] D. Lee, T. Minko, Nanotherapeutics for nose-to-brain drug delivery: an approach to bypass the blood brain barrier, Pharmaceutics 13 (2021) 2049, https://doi.org/10.3390/pharmaceutics13122049.
[10] N.N. Kumar, M. Gautam, J.J. Lochhead, D.J. Wolak, V. Ithapu, V. Singh, R. G. Thorne, Relative vascular permeability and vascularity across different regions of the rat nasal mucosa: implications for nasal physiology and drug delivery, Sci. Rep. 6 (2016) 31732, https://doi.org/10.1038/srep31732.
[11] A.E.-E. Aly, B. Harmon, L. Padegimas, O. Sesenoglu-Laird, M.J. Cooper, D. M. Yurek, B.L. Waszczak, Intranasal delivery of hGDNF plasmid DNA nanoparticles results in long-term and widespread transfection of perivascular cells in rat brain, Nanomedicine 16 (2019) 20–33, https://doi.org/10.1016/j.nano.2018.11.006.
[12] M.L. Formica, D.A. Real, M.L. Picchio, E. Catlin, R.F. Donnelly, A.J. Paredes, On a highway to the brain: a review on nose-to-brain drug delivery using nanoparticles, Appl. Mater. Today 29 (2022) 101631, https://doi.org/10.1016/j.apmt.2022.101631.
[13] G. Barbato, R. Nisticò, V. Triaca, Exploiting focused ultrasound to aid intranasal drug delivery for brain therapy, Front. Pharmacol. 13 (2022) 786475, https://doi.org/10.3389/fphar.2022.786475.
[14] W.-Y. Chai, P.-C. Chu, M.-Y. Tsai, Y.-C. Lin, J.-J. Wang, K.-C. Wei, Y.-Y. Wai, H.-L. Liu, Magnetic-resonance imaging for kinetic analysis of permeability changes during focused ultrasound-induced blood-brain barrier opening and brain drug delivery, J. Contr. Release 192 (2014) 1–9, https://doi.org/10.1016/j.jconrel.2014.06.023.
[15] P.-Y. Chen, H.-Y. Hsieh, C.-Y. Huang, C.-Y. Lin, K.-C. Wei, H.-L. Liu, Focused ultrasound-induced blood-brain barrier opening to enhance interleukin-12 delivery for brain tumor immunotherapy: a preclinical feasibility study, J. Transl. Med. 13 (2015) 93, https://doi.org/10.1186/s12967-015-0451-y.
[16] H. Chen, C.C. Chen, C. Acosta, S.-Y. Wu, T. Sun, E.E. Konofagou, A new brain drug delivery strategy: focused ultrasound-enhanced intranasal drug delivery, PLoS One 9 (2014), e108880, https://doi.org/10.1371/journal.pone.0108880.
[17] D. Ye, X. Zhang, Y. Yue, R. Raliya, P. Biswas, S. Taylor, Y.-C. Tai, J.B. Rubin, Y. Liu, H. Chen, Focused ultrasound combined with microbubble-mediated intranasal delivery of gold nanoclusters to the brain, J. Contr. Release 286 (2018) 145–153, https://doi.org/10.1016/j.jconrel.2018.07.020.
[18] P.N. Hanieh, C. Ricci, A. Bettucci, R. Marotta, C.M. Moran, L. Cantù, M. Carafa, F. Rinaldi, E. Del Favero, C. Marianecci, Ultrastable shelled PFC nanobubbles: a platform for ultrasound-assisted diagnostics, and therapy, Nanomed. Nanotechnol. Biol. Med. 46 (2022) 102611, https://doi.org/10.1016/j.nano.2022.102611.
[19] Y. Negishi, M. Yamane, N. Kurihara, Y. Endo-Takahashi, S. Sashida, N. Takagi, R. Suzuki, K. Maruyama, Enhancement of blood–brain barrier permeability and delivery of antisense oligonucleotides or plasmid DNA to the brain by the combination of bubble liposomes and high-intensity focused ultrasound, Pharmaceutics 7 (2015) 344–362, https://doi.org/10.3390/pharmaceutics7030344.
[20] C.-Y. Lin, W.G. Pitt, Acoustic droplet vaporization in biology and medicine, BioMed Res. Int. 2013 (2013) 404361, https://doi.org/10.1155/2013/404361.
[21] G. Serbest, J. Horwitz, M. Jost, K.A. Barbee, Mechanisms of cell death and neuroprotection by poloxamer 188 after mechanical trauma, Faseb. J. 20 (2006) 308–310, https://doi.org/10.1096/fj.05-4024fje.
[22] A. Pitto-Barry, N.P.E. Barry, Pluronic® block-copolymers in medicine: from chemical and biological versatility to rationalisation and clinical advances, Polym. Chem. 5 (2014) 3291–3297, https://doi.org/10.1039/C4PY00039K.
[23] K.C. De Castro, J.C. Coco, É.M. Dos Santos, J.A. Ataide, R.M. Martinez, M.H.M. Do Nascimento, J. Prata, P.R.M.L. Da Fonte, P. Severino, P.G. Mazzola, A.R. Baby, E. B. Souto, D.R. De Araujo, A.M. Lopes, Pluronic® triblock copolymer-based nanoformulations for cancer therapy: a 10-year overview, J. Contr. Release 353 (2023) 802–822, https://doi.org/10.1016/j.jconrel.2022.12.017.
[24] D. Katti, Seth, A one-step electrospray-based technique for modulating morphology and surface properties of poly(lactide-co-glycolide) microparticles using Pluronics®, IJN (2012) 5129, https://doi.org/10.2147/IJN.S34185.
[25] O. Kontogiannis, D. Selianitis, D.R. Perinelli, G. Bonacucina, N. Pippa, M. Gazouli, S. Pispas, Non-ionic surfactant effects on innate pluronic 188 behavior: interactions, and physicochemical and biocompatibility studies, IJMS 23 (2022) 13814, https://doi.org/10.3390/ijms232213814.
[26] D.M. Nascimento, J.P. Macedo, A.M. Nascimento, Influência do Parâmetro de Equilíbrio Hidrofílico- Hidrofóbico (HLB) dos Polímeros F98 e F127 na eficácia da formação de nanopartículas de ouro e encapsulamento do fármaco capecitabina para tratamento de câncer de estomâgo, RSD 11 (2022), e43111334985, https://doi.org/10.33448/rsd-v11i13.34985.
[27] D. Ag Seleci, M. Seleci, J.-G. Walter, F. Stahl, T. Scheper, Niosomes as nanoparticular drug carriers: fundamentals and recent applications, J. Nanomater. 2016 (2016) 1–13, https://doi.org/10.1155/2016/7372306.
[28] R. Haj-Ahmad, A. Elkordy, C. Chaw, In vitro characterisation of Span™ 65 niosomal formulations containing proteins, CDD 12 (2015) 628–639, https://doi.org/10.2174/1567201812666150511095432.
[29] M.A. Carluccio, M. Massaro, C. Bonfrate, L. Siculella, M. Maffia, G. Nicolardi, A. Distante, C. Storelli, null De CaterinaR, Oleic acid inhibits endothelial activation : a direct vascular antiatherogenic mechanism of a nutritional component in the mediterranean diet, Arterioscler. Thromb. Vasc. Biol. 19 (1999) 220–228, https://doi.org/10.1161/01.atv.19.2.220.
[30] T.V.P. Bliss, G.L. Collingridge, A synaptic model of memory: long-term potentiation in the hippocampus, Nature 361 (1993) 31–39, https://doi.org/10.1038/361031a0.
[31] C. Marianecci, D. Paolino, C. Celia, M. Fresta, M. Carafa, F. Alhaique, Non-ionic surfactant vesicles in pulmonary glucocorticoid delivery: characterization and interaction with human lung fibroblasts, J. Contr. Release 147 (2010) 127–135, https://doi.org/10.1016/j.jconrel.2010.06.022.
[32] R. Corsaro, R. Lombardo, C. Ghelardini, L. Di Cesare Mannelli, D. Bani, A. Bonaccorso, R. Pignatello, Development of Eudragit® nanoparticles for intranasal drug delivery: preliminary technological and toxicological evaluation, Appl. Sci. 12 (2022) 2373, https://doi.org/10.3390/app12052373.
[33] D.M. Anderson, L.L. Hall, A.R. Ayyalapu, V.R. Irion, M.H. Nantz, J.G. Hecker, Stability of mRNA/cationic lipid lipoplexes in human and rat cerebrospinal fluid: methods and evidence for nonviral mRNA gene delivery to the central nervous system, Hum. Gene Ther. 14 (2003) 191–202, https://doi.org/10.1089/10430340360535751.
[34] B.R. Lentz, Membrane "fluidity" as detected by diphenylhexatriene probes, Chem. Phys. Lipids 50 (1989) 171–190, https://doi.org/10.1016/0009-3084(89)90049-2.
[35] J.J. Leskinen, K. Hynynen, Study of factors affecting the magnitude and nature of ultrasound exposure with in vitro set-ups, Ultrasound Med. Biol. 38 (2012) 777–794, https://doi.org/10.1016/j.ultrasmedbio.2012.01.019.
[36] M. Kinoshita, K. Hynynen, Key factors that affect sonoporation efficiency in in vitro settings: the importance of standing wave in sonoporation, Biochem. Biophys. Res. Commun. 359 (2007) 860–865, https://doi.org/10.1016/j.bbrc.2007.05.153.
[37] K. Hensel, M.P. Mienkina, G. Schmitz, Analysis of ultrasound fields in cell culture wells for in vitro ultrasound therapy experiments, Ultrasound Med. Biol. 37 (2011) 2105–2115, https://doi.org/10.1016/j.ultrasmedbio.2011.09.007.
[38] J.L. Rose, Ultrasonic Guided Waves in Solid Media, first ed., Cambridge University Press, 2014 https://doi.org/10.1017/CBO9781107273610.
[39] D. Mango, F. Weisz, R. Nisticò, Ginkgolic acid protects against aβ-induced synaptic dysfunction in the Hippocampus, Front. Pharmacol. 7 (2016), https://doi.org/10.3389/fphar.2016.00401.
[40] S. Shaarani, S. Hamid, N. Mohd Kaus, The Influence of pluronic F68 and F127 nanocarrier on physicochemical properties, in vitro release, and antiproliferative activity of thymoquinone drug, Phcog Res 9 (2017) 12, https://doi.org/10.4103/0974-8490.199774.
[41] M.M. Migliore, T.K. Vyas, R.B. Campbell, M.M. Amiji, B.L. Waszczak, Brain delivery of proteins by the intranasal route of administration: a comparison of cationic liposomes versus aqueous solution formulations, J Pharm Sci 99 (2010) 1745–1761, https://doi.org/10.1002/jps.21939.
[42] M. Danaei, M. Dehghankhold, S. Ataei, F. Hasanzadeh Davarani, R. Javanmard, A. Dokhani, S. Khorasani, M. Mozafari, Impact of particle size and polydispersity index on the clinical applications of lipidic nanocarrier systems, Pharmaceutics 10 (2018) 57, https://doi.org/10.3390/pharmaceutics10020057.
[43] F. Rinaldi, E. Del Favero, J. Moeller, P.N. Hanieh, D. Passeri, M. Rossi, L. Angeloni, I. Venditti, C. Marianecci, M. Carafa, I. Fratoddi, Hydrophilic silver nanoparticles loaded into niosomes: physical–chemical characterization in view of biological applications, Nanomaterials 9 (2019) 1177, https://doi.org/10.3390/nano9081177.
[44] J. Cauzzo, M. Nystad, A.M. Holsæter, P. Basnet, N. Škalko-Basnet, Following the fate of dye-containing liposomes in vitro, IJMS 21 (2020) 4847, https://doi.org/10.3390/ijms21144847.
[45] M. Frenzel, A. Steffen-Heins, Whey protein coating increases bilayer rigidity and stability of liposomes in food-like matrices, Food Chem. 173 (2015) 1090–1099, https://doi.org/10.1016/j.foodchem.2014.10.076.
[46] D. Ghernaout, Brownian motion and coagulation process, AJEP 4 (2015) 1, https://doi.org/10.11648/j.ajeps.s.2015040501.11.
[47] S. Bhattacharjee, DLS and zeta potential – what they are and what they are not? J. Contr. Release 235 (2016) 337–351, https://doi.org/10.1016/j.jconrel.2016.06.017.
[48] P. Nakhaei, R. Margiana, D.O. Bokov, W.K. Abdelbasset, M.A. Jadidi Kouhbanani, R.S. Varma, F. Marofi, M. Jarahian, N. Beheshtkhoo, Liposomes: structure, biomedical applications, and stability parameters with emphasis on cholesterol, Front. Bioeng. Biotechnol. 9 (2021) 705886, https://doi.org/10.3389/fbioe.2021.705886.
[49] A. Biagioni, A. Bettucci, D. Passeri, A. Alippi, Thermal Dependence of Ultrasound Contrast Agents Scattering Efficiency for Echographic Imaging Techniques, in: Rome, Italy, 2015, https://doi.org/10.1063/1.4922571, 020015.
[50] J.S. De Maar, C. Rousou, B. Van Elburg, H.J. Vos, G.P.R. Lajoinie, C. Bos, C.T. W. Moonen, R. Deckers, Ultrasound-Mediated drug delivery with a clinical

ultrasound system: in vitro evaluation, Front. Pharmacol. 12 (2021) 768436, https://doi.org/10.3389/fphar.2021.768436.
[51] K. Nigam, A. Kaur, A. Tyagi, M. Nematullah, F. Khan, R. Gabrani, S. Dang, Nose-to-brain delivery of lamotrigine-loaded PLGA nanoparticles, Drug Deliv. and Transl. Res. 9 (2019) 879–890, https://doi.org/10.1007/s13346-019-00622-5.
[52] F. Rinaldi, P. Hanieh, L. Chan, L. Angeloni, D. Passeri, M. Rossi, J. Wang, A. Imbriano, M. Carafa, C. Marianecci, Chitosan glutamate-coated niosomes: a proposal for nose-to-brain delivery, Pharmaceutics 10 (2018) 38, https://doi.org/10.3390/pharmaceutics10020038.
[53] V. Sharma, S. Anandhakumar, M. Sasidharan, Self-degrading niosomes for encapsulation of hydrophilic and hydrophobic drugs: an efficient carrier for cancer multi-drug delivery, Mater. Sci. Eng. C 56 (2015) 393–400, https://doi.org/10.1016/j.msec.2015.06.049.
[54] Prepared by the Safety Group of the British Medical Ultrasound Society, Guidelines for the safe use of diagnostic ultrasound equipment, Ultrasound 18 (2010) 52–59, https://doi.org/10.1258/ult.2010.100003.
[55] R.E. Apfel, C.K. Holland, Gauging the likelihood of cavitation from short-pulse, low-duty cycle diagnostic ultrasound, Ultrasound Med. Biol. 17 (1991) 179–185, https://doi.org/10.1016/0301-5629(91)90125-G.
[56] F. Ahmadi, I.V. McLoughlin, A new mechanical index for gauging the human bioeffects of low frequency ultrasound, Annu Int Conf IEEE Eng Med Biol Soc 2013 (2013) 1964–1967, https://doi.org/10.1109/EMBC.2013.6609913.
[57] J.D. Marks, C.Y. Pan, T. Bushell, W. Cromie, R.C. Lee, Amphiphilic, tri-block copolymers provide potent membrane-targeted neuroprotection, Faseb. J. 15 (2001) 1107–1109, https://doi.org/10.1096/fj.00-0547fje.
[58] M. Di Maso, W.C. Purdy, S.A. McClintock, M.L. Cotton, Determination of sorbitan trioleate in metered-dose inhalers by supercritical-fluid chromatography, J. Pharmaceut. Biomed. Anal. 8 (1990) 303–305, https://doi.org/10.1016/0731-7085(90)80042-N.